Magnetoelasticity of dilute Cr-Si alloy single crystals

1993 J. Phys.: Condens. Matter 5 1733

(http://iopscience.iop.org/0953-8984/5/11/013)

J. Phys.: Condens. Matter 5 (1993) 1733–1752. Printed in the UK

Magnetoelasticity of dilute Cr–Si alloy single crystals

R A Anderson†, H L Alberts and P Smit

Department of Physics, Rand Afrikaans University, P O Box 524, Auckland Park, Johannesburg 2006, South Africa

Received 12 November 1992, in final form 13 January 1993

Abstract. Measurements are reported of the temperature dependence of the elastic constants and thermal expansion of dilute Cr–Si alloy single crystals containing 0.5, 1.2, 1.6 and 3.0 at.% Si. Well defined anomalies in all elastic constants, and in the thermal expansion, were observed at the Néel points (T_N) and at the commensurate–incommensurate spin density wave transition temperatures (T_{IC}) of the alloys. Elastic anomalies were also observed at the longitudinal–transverse incommensurate spin density wave transition temperature of the Cr + 0.5 at.% Si crystal, but not in the thermal expansion thereof. The transition at the Néel point of the Cr + 0.5 at.% Si crystal is continuous, that of the Cr + 1.2 at.% Si and Cr + 1.6 at.% Si crystals of first order, while the order of the transition in the Cr + 3.0 at.% Si crystal could not be determined unambiguously. For the Cr + 1.2 at.% Si and Cr + 1.6 at.% Si crystals the discontinuous transitions at T_N show hysteresis behaviour. In the 1.2 at.% Si crystal it is also accompanied by structure effects that were absent for 1.6 at.% Si. Hysteresis, accompanied by structure effects, was also observed at T_{IC} for Cr + 1.2 at.% Si. The structure effects are ascribed to the possibility of mixed incommensurate–commensurate spin density wave states in the dilute Cr–Si magnetic phase diagram. The magnetovolume and magnetic contributions to the bulk modulus have been found to fit the equation $a + bT^2 + cT^4$, predicted by theory, rather well up to temperatures (T) close to the Neél points of Cr + 0.5 at.% Si and Cr + 1.6 at.% Si.

1. Introduction

The magnetic phase diagram of the dilute Cr–Si alloy system is complex [1]. It consists of a commensurate (C) spin density wave (SDW) region, an incommensurate (I) SDW region appearing at low Si concentrations, and a paramagnetic (P) region. A triple point exists near 1 at.% Si and 230 K, where the above three states coexist. There is a further remarkable feature in the magnetic phase diagram: it has [2] a re-entrant CSDW phase in the vicinity of the triple point. This feature is unique among Cr binary alloys containing non-transition metals. The magnetic phase diagram [1] of Cr–Ge alloys, for instance, behaves normally, without any re-entrant feature. Indirect evidence for the re-entrant feature in the magnetic phase diagram of the Cr–Si alloy system was obtained by Mizuki and co-workers [2] from neutron diffraction experiments on a Cr + 0.85 at.% Si single crystal. A change in sign was observed for dQ/dT, where Q is the SDW wavevector, of Cr + 0.85 at.% Si at a temperature $T = 230$ K, which lies below the Néel point, $T_N = 258$ K. This alloy has a

† Permanent address: Department of Physics, University of Western Australia, Nedlands WA 6009, Australia.

0953-8984/93/111733+20$07.50

concentration just lower than the triple-point concentration and remains in the ISDW phase for $T < T_N$. For 230 K $< T < T_N$, dQ/dT is positive, the ISDW phase becomes more 'commensurate' as the temperature is lowered from T_N to 230 K, and for $T < 230$ K, dQ/dT is negative. From these observations Mizuki and co-workers [2] suggest a re-entrant CSDW region in the magnetic phase diagram of Cr–Si alloys between 0.85 and 1.4 at.% Si, giving rise to an I–C–I–P sequence of transitions as the temperature increases from 0 K in this concentration range.

However, careful measurements [3] of the magnetoelastic properties of polycrystalline Cr–Si alloys close to the triple point show no effects of the re-entrant feature. One reason for this is probably the fact that the expected C → I and I → P transition temperatures in the re-entrant region are too close (≈ 10 K) together to be resolved by magnetoelastic measurements. A further complication in observing the re-entrant phase is due to the fact that no anomaly was observed [3] in either the bulk-modulus or the shear elastic constant at the I → C phase transition of polycrystalline Cr–Si alloys.

On the other hand, sharp anomalies were recently observed [4] at T_{IC} in all elastic constants of a Cr + 0.3 at.% Ru single crystal. As far as we are aware, this was the first such study on dilute Cr alloy single crystals. Other dilute Cr alloy single crystals with I → C transitions should therefore also be studied to ascertain whether the elastic anomalies observed at T_{IC} of the Cr + 0.3 at.% Ru crystal are a common feature of all Cr alloy single crystals. This is particularly so for dilute Cr–Si alloys, for which the polycrystalline elastic constants show no anomaly at T_{IC} and of which the single-crystal elastic constants have not yet been studied. Searching for evidence of the existence of the re-entrant CSDW phase in the Cr–Si alloy system from the behaviour of the elastic constants should be more appropriate through studies on single crystals than on polycrystalline material. A study on Cr–Si single crystals should furthermore provide valuable information concerning the first-order C → P transition observed in Cr–Si alloys at T_N for concentrations above the triple-point concentration.

We report a detailed study of the elastic constants and thermal expansion of dilute Cr–Si alloy single crystals. Well defined anomalies were observed in all elastic constants at T_{IC} in single-crystal alloys, although such anomalies were absent in the previous studies on polycrystalline material.

2. Experimental procedure

Single crystals of dilute Cr–Si alloys containing 0.5, 1.2, 1.6 and 3.0 at.% Si were grown by a floating-zone technique using RF heating in a pure argon atmosphere. A bar of the alloy, roughly cylindrical in form, of length between 10–15 cm and diameter between 7–10 mm was first prepared by RF melting in a horizontal cold crucible. This bar was then grown into a single crystal of length about 5 cm and diameter about 6 mm by the floating-zone technique with the bar in a vertical position. The starting materials were 99.996% pure iochrome and 99.999% pure Si. Electron microprobe analysis at different positions on the crystals shows that they are homogeneous to within less than 5% of the quoted concentration and that the actual concentration differs on the average by about 6% from the above quoted nominal concentrations. The crystals were prepared for the ultrasonic measurements with parallel (100) and (110) faces by spark planing. Distances between these parallel faces were of the order of 6 mm, and the surface areas were about 25–30 mm^3.

Ultrasonic (10 MHz) wave velocities were determined using either a phase comparison method [5] or, in some instances, the pulse-echo overlap technique [6], depending upon which equipment produced the best signals for measurement. The sensitivity of the former technique was about 1 part in 10^3 or better, and of the latter about 1 part in 10^5. The error in the absolute values of the sound velocity is about 0.5%. As previously described [7], thermal-expansion measurements were made using a strain gauge technique. Measurements were made relative to Cr + 5 at.% V, which remains paramagnetic at all temperatures and serves to simulate [8] the non-magnetic component of the Cr–Si alloys, i.e. $(\Delta L/L)_{\text{meas}} = (\Delta L/L)_{\text{Cr-V}} - (\Delta L/L)_{\text{Cr-Si}}$. Thermal-expansion measurements were made either along the [100] or [110] directions. The error in the absolute values of $\Delta L/L$ is about 5%, while changes of 3×10^{-7} could be detected easily.

All ultrasonic measurements were done in the temperature range 77–500 K by heating the sample slowly at a rate of about 0.6 K per minute. For detailed measurements close to the transition temperatures the heating rate was about 3 K per hour and the measurements were done at 0.01–0.05 K intervals. For some samples, measurements were also done on the cooling cycle to check for hysteresis effects. In the case of the thermal-expansion measurements, data were recorded at 0.05 K intervals during cooling runs and at 0.005 K during heating runs, which was done at a rate of about 0.06 K per minute in the proximity of the transition.

3. Results

3.1. Elastic constants

The elastic constants were obtained from the ultrasonic wave velocities and densities by using the standard equations [9] for cubic crystals. Densities were calculated from the lattice parameters of the alloys, which decrease by about 0.015% per at.% solute added [10]. The effects of thermal expansion have been neglected in calculating the elastic constants. Thermal expansion measurements reported in the next section show that at 77 K the correction amounts to about 0.05%, and is too small to affect the data significantly. The discontinuity ($\Delta L/L \approx 5 \times 10^{-4}$) in thermal expansion at T_N for the alloys showing a first-order C–P transition, are furthermore also insignificant in affecting the longitudinal modes c_{11} and c_L at T_N. This discontinuity does, however, contribute in part to the anomalies observed at T_N in the shear constants.

The temperature dependences of the elastic constants c_{11}, $c_L = \frac{1}{2}(c_{11} + c_{12} + 2c_{44})$, $c' = \frac{1}{2}(c_{11} - c_{12})$ and c_{44} are shown for Cr + 0.5 at.% Si, Cr + 1.2 at.% Si, Cr + 1.6 at.% Si and Cr + 3.0 at.% Si, respectively, in figures 1, 2, 3 and 4. Due to large attenuation of the ultrasonic waves for the c_L mode in the Cr + 3.0 at.% Si crystal, c_L was not measured for this crystal. For the c_{11} mode in the latter crystal very large attenuation was also observed in the CSDW phase below T_N, although absent above T_N, to such an extent that measurements of c_{11} below T_N could not be done. These attenuation problems were absent for the shear modes in this crystal. In general, very good ultrasonic echoes were observed in the Cr–Si single crystals except for very large attenuation effects of the longitudinal modes in the CSDW phase, becoming largest for the Cr + 3.0 at.% Si crystal, thereby hampering measurements of c_{11} in its CSDW phase. These attenuation effects were absent in the ISDW or P phases of the crystals. The high attenuation for the longitudinal modes c_{11} and c_L, usually observed in Cr

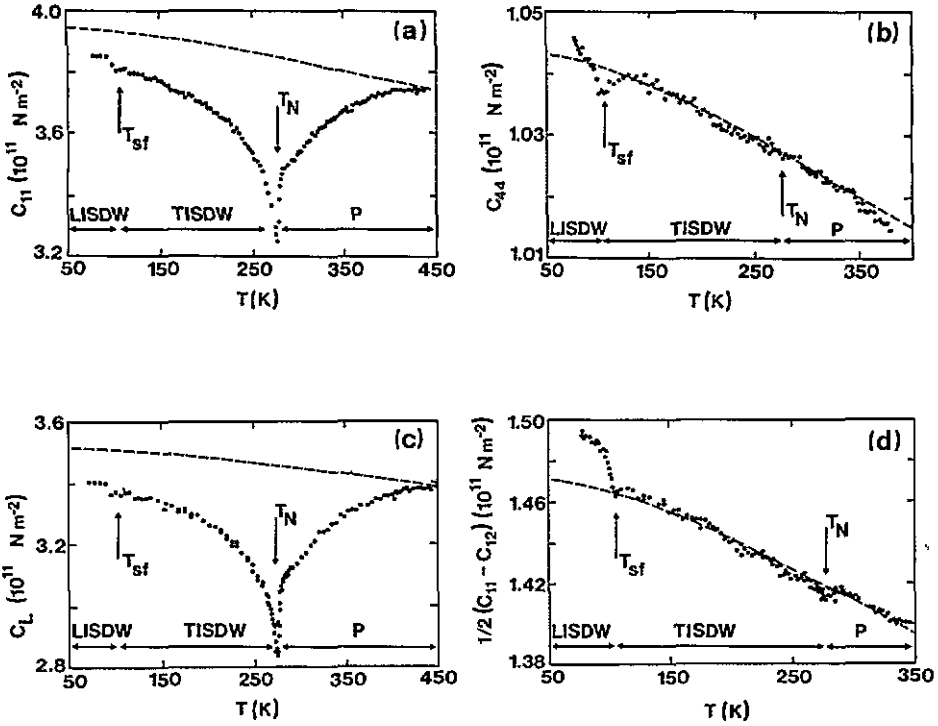

Figure 1. Elastic constants of Cr + 0.5 at.% Si as a function of temperature. (*a*) c_{11}, (*b*) c_{44}, (*c*) $c_L = \frac{1}{2}(c_{11} + c_{12} + 2c_{44})$ and (*d*) $\frac{1}{2}(c_{11} - c_{12})$. For clarity, only one out of every eight points measured is plotted. The broken curves are the expected non-magnetic behaviour determined from results of Cr + 5 at.% V.

and its alloys close to T_N for the ISDW-P transition, was also observed in the Cr + 0.5 at.% Si single crystal. Although large at T_N, the attenuation was however such that the ultrasonic echoes were good at all temperatures and all elastic constants could be followed continuously through T_N for Cr + 0.5 at.% Si. For the crystals (1.2 at.% Si, 1.6 at.% Si and 3.0 at.% Si) showing CSDW-P transitions at T_N however, the attenuation for the c_L and c_{11} modes became so high at T_N that the ultrasonic echoes were lost in a small temperature range around T_N for Cr + 1.2 at.% Si and Cr + 1.6 at.% Si and were completely lost at all temperatures below T_N for c_{11} of Cr + 3.0 at.% Si. In the case of the shear modes, the magnetic states of the crystals do not have such a large effect on the ultrasonic attenuation. Table 1 summarizes the anomalies observed at T_{sf}, T_{IC} and T_N, T_{sf} being the spin-flip transition temperature where the transverse (T) ISDW phase transforms to a longitudinal (L) ISDW phase.

As in previous work [3, 7], the temperature dependence of the elastic constants of a Cr + 5 at.% V single crystal, which remains paramagnetic at all temperatures, was used as a reference for the expected temperature dependence of the non-magnetic behaviour of the Cr–Si single crystals. The curves for Cr + 5 at.% V [8] of the corresponding elastic constants in figures 1, 2, 3 and 4 were shifted slightly up or down to coincide as closely as possible with the high-temperature measurements of the Cr–Si crystals. These curves are shown by the broken curves in figures 1, 2, 3 and 4. Except for $\frac{1}{2}(c_{11} - c_{12})$ of the Cr + 3.0 at.% Si crystal, the data for the temperature dependence of the shear modes above T_N of the Cr–Si crystals are well

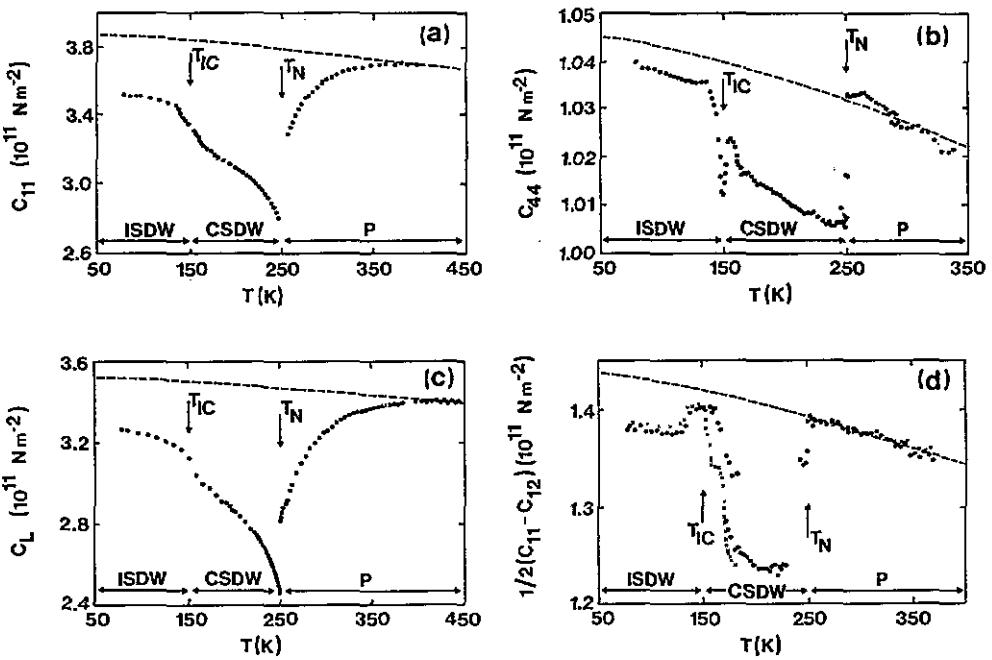

Figure 2. Elastic constants of Cr + 1.2 at.% Si as a function of temperature. (*a*) c_{11}, (*b*) c_{44}, (*c*) $c_L = \frac{1}{2}(c_{11} + c_{12} + 2c_{44})$ and (*d*) $\frac{1}{2}(c_{11} - c_{12})$. Points • were measured using the phase comparison method and points × using the pulse echo overlap method. In (*c*) and (*d*) every second point is plotted for clarity, in (*a*) only one out of every eight points measured and in (*b*) all the points are plotted. The broken curves are the expected non-magnetic behaviour determined from results of Cr + 5 at.% V.

represented by that of Cr + 5 at.% V. Magnetic effects persist in the longitudinal modes, c_{11} and c_L, of the Cr–Si crystals up to relatively high temperatures above T_N. The magnetic contributions

$$\Delta C = C_{Cr_{95}V_5} - C_{Cr-Si}$$

to the elastic constants are obtained by subtracting the measured values for the Cr–Si crystals from the broken curves in figures 1, 2, 3 and 4.

Figure 5 shows the temperature dependence of the adiabatic bulk modulus $B = c_L - c_{44} - c'/3$ for Cr + 0.5 at.% Si, Cr + 1.2 at.% Si and Cr + 1.6 at.% Si. ΔB, Δc_L and Δc_{11} obtained from figures 1, 2, 3 and 5 behave very similarly, showing much larger magnetic effects for the longitudinal modes than for the shear modes when the crystal is cooled through T_N. This was previously also found for pure Cr [11] and for other Cr alloys [1], for which magnetic effects in the shear modes are negligibly small. As can be seen in figure 1, shear effects are also negligibly small for the TISDW phase of Cr + 0.5 at.% Si, showing within the experimental error no magnetic effects down to T_{sf} when cooled through T_N. Below T_{sf}, in the LISDW phase, the magnetic contributions to the shear constants of this crystal are less than 2% (figure 1). For the Cr + 1.2 at.% Si crystal, magnetic contributions to the shear constants in the CSDW phase are larger than in the ISDW phase of the crystal. In the CSDW phase between T_{IC} and T_N of this crystal, there is approximately a 2.4 % magnetic contribution to c_{44} and a 12% contribution to $\frac{1}{2}(c_{11} - c_{12})$, compared to

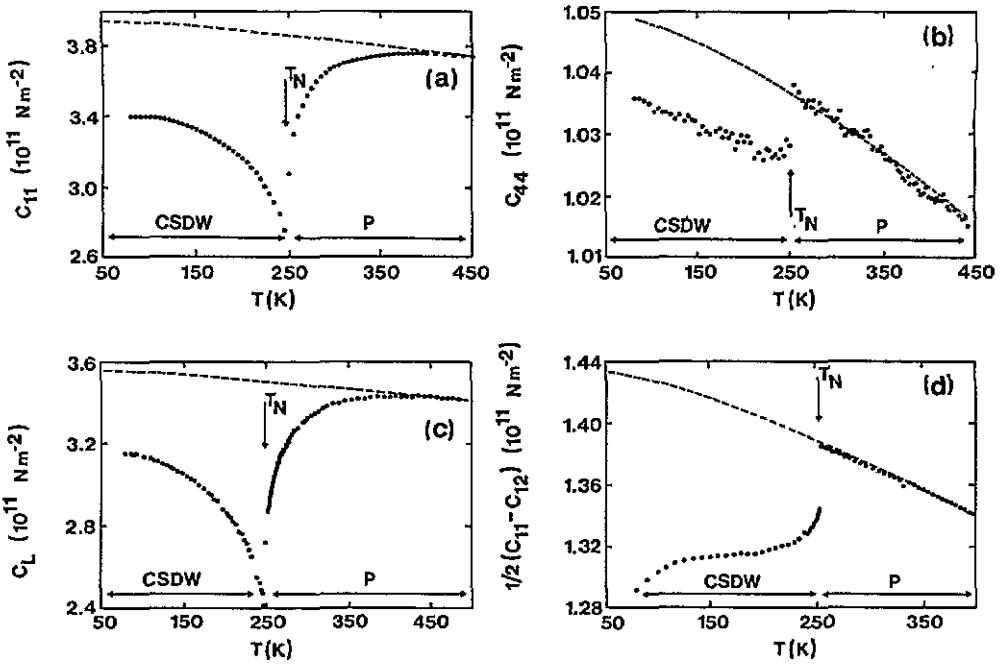

Figure 3. Elastic constants of Cr + 1.6 at.% Si as a function of temperature. (*a*) c_{11}, (*b*) c_{44}, (*c*) $c_L = \frac{1}{2}(c_{11} + c_{12} + 2c_{44})$ and (*d*) $\frac{1}{2}(c_{11} - c_{12})$. For clarity only every third point is plotted in (*a*) and (*c*), only every fourth point in (*b*) and every second point in (*d*). The broken curves are the expected non-magnetic behaviour determined from results of Cr + 5 at.% V.

contributions of respectively 0.6% and 4% in the ISDW phase below T_{IC}. On the other hand, in the case of the longitudinal-mode constants c_{11} and c_L of Cr + 1.2 at.% Si, the magnetic contributions in the CSDW phase vary between 18% near T_{IC} and 45% near T_N, while it is approximately 10% below T_{IC} in the ISDW phase. Magnetic effects in the longitudinal-mode constants in the CSDW phase of this crystal thus also dominate the shear effects, but to a lesser extent than for Cr + 0.5 at.% Si. This was also found for the CSDW phase of the Cr + 1.6 at.% Si crystal. Volume effects therefore seem to be dominant in the magnetoelastic coupling of dilute Cr–Si alloys, as is also the case in pure Cr and other dilute Cr alloys [1].

As shown in figure 2, a reproducible structure was observed in the temperature behaviour of c_{44} and $\frac{1}{2}(c_{11} - c_{12})$ near T_{IC} and T_N of Cr + 1.2 at.% Si. This structure is very prominent near T_{IC} and is shown to a lesser extent also for c_{11}. It occurs within a temperature range of about 35 K around $T_{IC} \approx 150$ K for all three modes. In the case of $\frac{1}{2}(c_{11} - c_{12})$ both pulse-echo overlap and phase comparison measurements are shown near T_{IC} in figure 2, showing the structure very clearly. The structure in the shear constants at T_N is not so clear in figure 2, where only every second point is plotted for clarity. The detailed measurements of $\frac{1}{2}(c_{11} - c_{12})$ on slowly heating the sample, however, show that the transition occurs near 250 K in two stages, within a temperature range of about 5 K. In the first stage, high attenuation results in a loss of the ultrasonic echoes between 248 K and 250 K, accompanied by a jump in $\frac{1}{2}(c_{11} - c_{12})$ between these two temperatures. At 250 K, halfway through the transition, the echos reappear in a small temperature range of about 1–2 K to

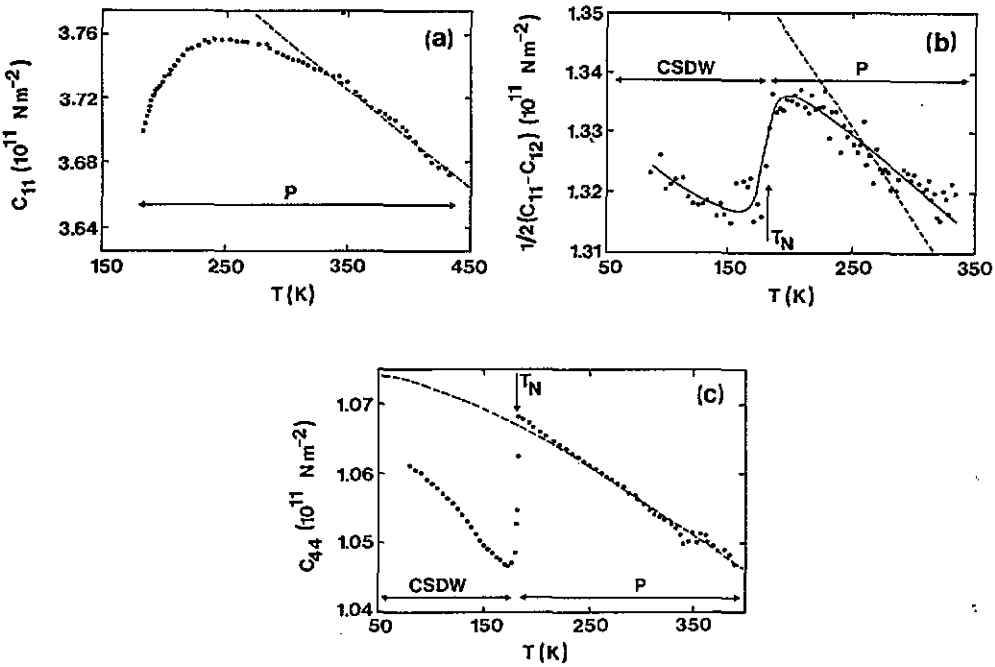

Figure 4. Elastic constants of Cr + 3.0 at.% Si as a function of temperature. (*a*) c_{11}, (*b*) $\frac{1}{2}(c_{11}-c_{12})$ and (*c*) c_{44}. For clarity only every second point is plotted in (*a*) and (*b*) and every fourth point in (*c*). The broken curves are the expected non-magnetic behaviour determined from results of Cr + 5 at.% V.

Table 1. Summary of the elastic constant anomalies observed at T_{sf}, T_{IC} and T_N.

Sample	Mode	Low-temperature anomaly at T_{sf}	Intermediate-temperature anomaly at T_{IC}	Higher-temperature anomaly at T_N
0.5 at.% Si	c_{11}	Small	IC transition not present	Large, continuous
	c_L	Small	IC transition not present	Large, continuous
	c_{44}	Small	IC transition not present	No anomaly
	$\frac{1}{2}(c_{11}-c_{12})$	Small	IC transition not present	Very small
1.2 at.% Si	c_{11}	—	Well defined with structure	Large, nearly discontinuous
	c_L	—	Well defined	Large, nearly discontinuous
	c_{44}	—	Sharp with structure	Nearly discontinuous
	$\frac{1}{2}(c_{11}-c_{12})$	—	Sharp with structure	Nearly discontinuous with structure
1.6 at.% Si	c_{11}	—	—	Large, nearly discontinuous
	c_L	—	—	Large, nearly discontinuous
	c_{44}	—	—	Small
	$\frac{1}{2}(c_{11}-c_{12})$	—	—	Small, nearly discontinuous
3.0 at.% Si	c_{11}	—	—	Attenuation too high to observe
	c_L	—	—	Attenuation too high to observe
	c_{44}	—	—	Small, nearly discontinuous
	$\frac{1}{2}(c_{11}-c_{12})$	—	—	Small

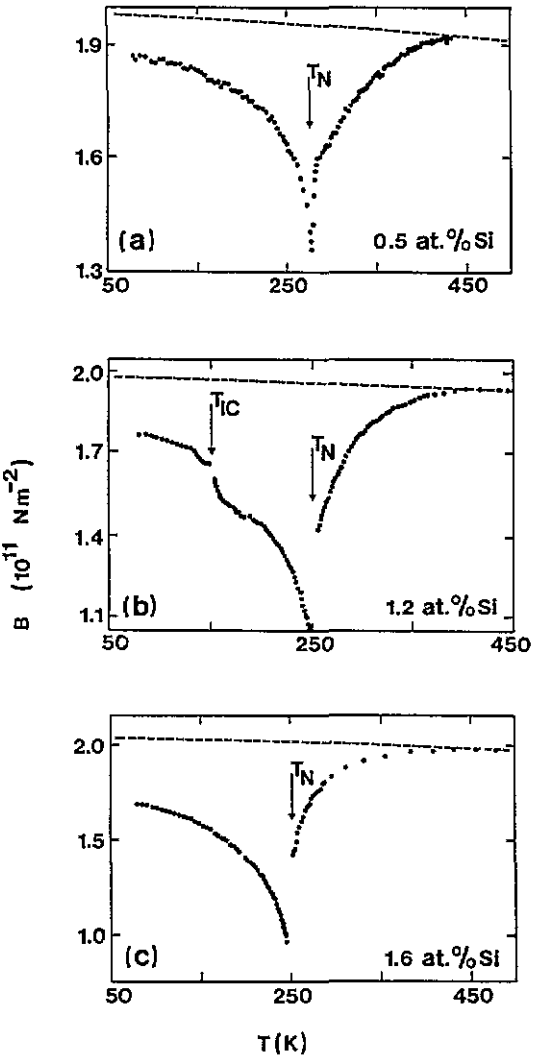

Figure 5. Temperature dependence of the adiabatic bulk modulus, B, as a function of temperature for (*a*) Cr + 0.5 at.% Si, (*b*) Cr + 1.2 at.% Si and (*c*) Cr + 1.6 at.% Si. The broken curves are the expected non-magnetic behaviour determined from results of Cr + 5 at.% V.

disappear again, due to high attenuation, in the second stage up to about 253 K. The second stage is again accompanied by a jump in $\frac{1}{2}(c_{11} - c_{12})$. Due to the very large attenuation, accompanied by a total loss of the ultrasonic echoes for the longitudinal modes near T_N, no structure could be observed in the behaviour of c_{11} or c_L for Cr + 1.2 at.% Si near T_N. Heating and cooling runs for c_L through T_N show a hysteresis effect of width about 7 K, as was also found in the thermal expansion measurements (see subsection 3.2), for this crystal.

In an initial study [12] on the longitudinal wave velocity along [110] of the Cr + 1.6 at.% Si crystal, we observed no hysteresis effects during heating and cooling runs through T_N. The high attenuation observed close to T_N for the longitudinal

modes in this crystal hampered an accurate observation of hysteresis effects in these modes at T_N, especially when the hysteresis effects are relatively small. A hysteresis effect of width about 3K, (compared to 7K observed in the thermal expansion measurements), however, was indeed observed for measurements of $\frac{1}{2}(c_{11}-c_{12})$, for which the attenuation problem at T_N is not that severe, during heating and cooling runs through T_N of the Cr + 1.6 at.% Si crystal.

The temperature T_N was taken at the sharp minima in the c_{11}–T or c_L–T curves in figures 1, 2 and 3 for Cr + 0.5 at.% Si, Cr + 1.2 at.% Si and Cr + 1.6 at.% Si, respectively. For the latter two crystals the sharp minima in c_{11} and c_L at T_N are accompanied by sharp, nearly discontinuous, step-like anomalies in c_{44} and $\frac{1}{2}(c_{11}-c_{12})$. For Cr + 3 at.% Si, for which c_{11} and c_L could not be measured below T_N, T_N was taken at the temperature of the nearly discontinuous change in c_{44} of figure 4. The I–C transition was only observed in the Cr + 1.2 at.% Si crystal. For this, T_{IC} was taken at the midpoint of the transition around 150 K on the c_{11}–T curve. The temperature T_{sf} was observed only for Cr + 0.5 at.% Si. It is characterized by small anomalies in the temperature dependence of all the elastic constants of this crystal, and T_{sf} is taken at the start of the sharp rise in $\frac{1}{2}(c_{11}-c_{12})$ that occurs with decreasing temperature. Elastic anomalies were not observed at T_{sf} for polycrystalline Cr + 0.5 at.% Si, nor at T_{IC} for any of the polycrystalline Cr–Si alloys studied in the previous work [3]. The transition temperatures obtained in the elastic constant measurements are shown in table 2 and are marked in figures 1, 2, 3 and 4. Figure 6(*a*) shows the detailed behaviour of c_{11} for the Cr + 0.5 at.% Si crystal around T_N. An interesting behaviour is the sharp change in slope at 282 K. Just below and above this temperature, c_{11} varies linearly with temperature. The reason for this behaviour is not known, but it may be mentioned that we observed similar behaviour in a pure Cr crystal for which the measurements are shown in figure 6(*b*).

Table 2. Transition temperatures T_{sf}, T_{IC} and T_N as determined from elastic-constant and thermal-expansion measurements on Cr–Si single crystals.

Sample	Method	T_{sf} (K)		T_{IC} (K)		T_N (K)	
		Heating	Cooling	Heating	Cooling	Heating	Cooling
0.5 at.% Si	Ultrasonics	105 ± 5	—	—	—	277 ± 2	—
0.5 at.% Si	Thermal expansion			—	—	278 ± 2	278 ± 2
1.2 at.% Si	Ultrasonics	—	—	150 ± 10	—	250 ± 2	—
1.2 at.% Si	Thermal expansion	—	—	Between 108–163	Between 77–145	252.8 ± 0.1	248.6 ± 0.1
1.6 at.% Si	Ultrasonics	—	—	—	—	252 ± 2	(249 ± 2)
1.6 at.% Si	Thermal expansion	—	—	—	—	252.94 ± 0.05	245.87 ± 0.05
3.0 at.% Si	Ultrasonics	—	—	—	—	182 ± 3	—
3.0 at.% Si	Thermal expansion	—	—	—	—	181 ± 4	—

3.2. Thermal expansion

The thermal expansion

$$(\Delta L/L)_{meas} \simeq (\Delta L/L)_{Cr_{95}V_5} - (\Delta L/L)_{Cr-Si}$$

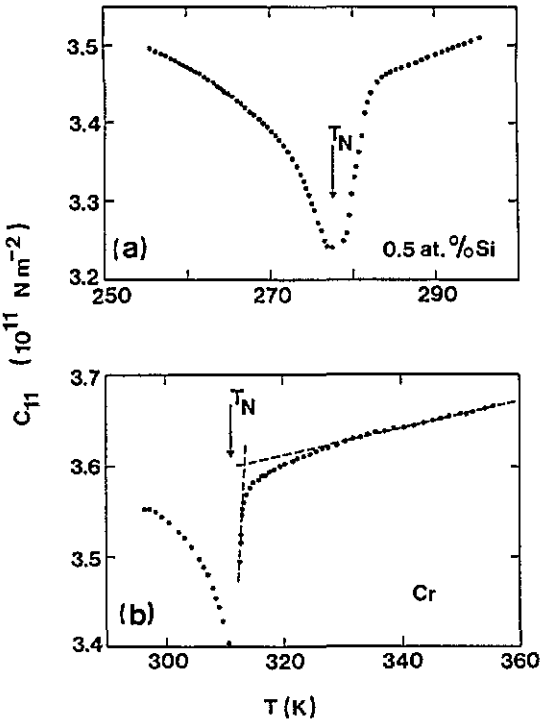

Figure 6. Detailed behaviour of c_{11} around the Néel point for (*a*) the Cr + 0.5 at.% Si crystal and (*b*) pure Cr.

measured along [100], is shown in figures 7(*a*), (*b*), (*c*) and (*d*) for 0.5 at.% Si, 1.2 at.% Si, 1.6 at.% Si and 3.0 at.% Si, respectively. Measurements were done during both cooling and heating runs. The term $(\Delta L/L)_{\text{meas}}$ varies continuously, with no hysteresis effects, through the Néel transition of Cr + 0.5 at.% Si, but is characterized by a sharp change in slope at (278 ± 2) K. This temperature was taken as T_N on the $\Delta L/L$–T curve. On the other hand, the Cr + 1.2 at.% Si and Cr + 1.6 at.% Si crystals show sharp discontinuous transitions in $(\Delta L/L)_{\text{meas}}$ at T_N that are accompanied by hysteresis effects, as shown in the detailed behaviour depicted in figures 8(*a*) and (*b*). The discontinuity for 1.2 at.% Si occurs within less than 1 K and that for 1.6 at.% Si in about 0.005 K, showing that these two crystals are of good quality and of good homogeneity. For Cr + 1.2 at.% Si the hysteresis width near T_N is about 4 K and for Cr + 1.6 at.% Si about 7 K. For the Cr + 3.0 at.% Si crystal, $(\Delta L/L)_{\text{meas}}$ shows very little hysteresis during heating and cooling measurements, except close to 177 K, where there is a small discontinuity and small hysteresis of width about 1 K, and close to 184 K where there is a similar hysteresis effect. In between these two temperatures $(\Delta L/L)_{\text{meas}}$ vary continuously with very little, if any, hysteresis effects (figure 8(*c*)). We conclude from the discussion above that the Néel transition for the 0.5 at.% Si crystal is second order and that of Cr + 1.2 at.% Si and Cr + 1.6 at.% Si is first order. The results for the 3.0 at.% Si crystal are not such as to give a straightforward answer on the order of the transition. For Cr + 1.2 at.% Si and Cr + 1.6 at.% Si, T_N was taken at the sharp discontinuities on the $(\Delta L/L)_{\text{meas}}$–$T$ curves and for Cr + 3.0 at.% Si it was taken at the small peak at

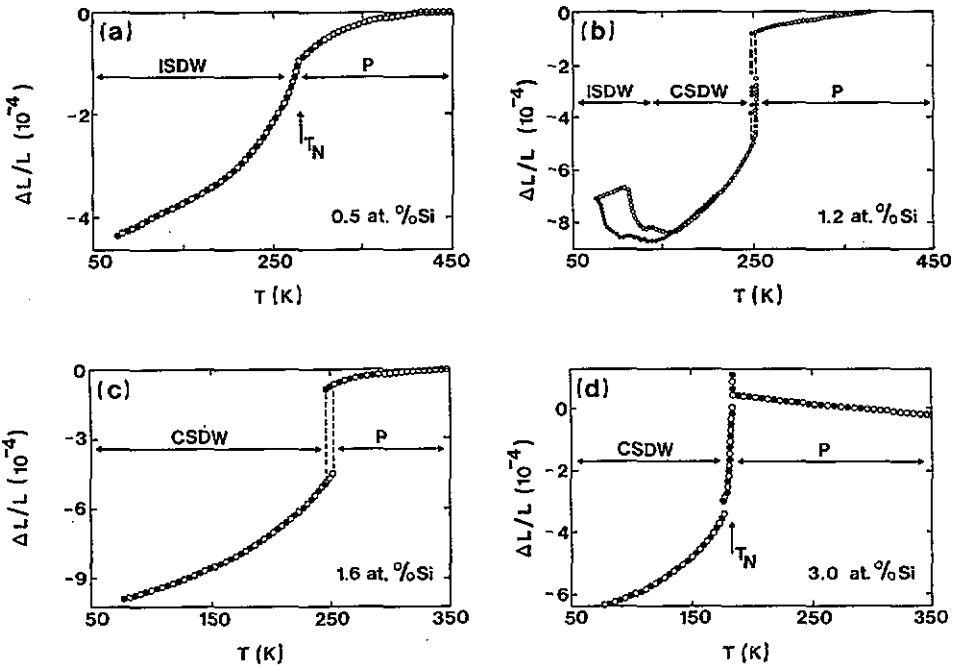

Figure 7. Temperature dependence of $\Delta L/L = (\Delta L/L)_{meas} = (\Delta L/L)_{Cr_{95}V_5} - (\Delta L/L)_{Cr-Si}$ measured along [100] for (*a*) Cr + 0.5 at.% Si, (*b*) Cr + 1.2 at.% Si, (*c*) Cr + 1.6 at.% Si and (*d*) Cr + 3.0 at.% Si. Points marked o were measured during heating and points marked • were measured during cooling. Measurements were recorded at temperature intervals smaller than 0.05 K on cooling and smaller than 0.005 K on heating. All the data points fall on smooth curves and only representative points are shown in the figures.

184 K, which coincides with T_N as obtained from the ultrasonic data. Values of T_N obtained from the thermal expansion measurements during both heating and cooling runs are also tabulated in table 2.

The I–C (on heating) and C–I (on cooling) transitions are marked by large anomalies, with hysteresis effects, on the $(\Delta L/L)_{meas}$–T curves of the Cr + 1.2 at.% Si crystal. The first of these transitions occurs in a temperature range between 77–145 K and the latter between 108–163 K (figure 8(*d*)). There is a reproducible structure in the transition region for each case. This in a sense reflects the structure effects observed at T_{IC} during the elastic-constant measurements of this crystal. We attribute the structure effects to the possibility of mixed ISDW/CSDW phases that may occur during the transition. Mixed ISDW/CSDW states were previously also reported [13] for other dilute Cr alloys near T_{IC}. The structure effects near T_{IC} were not previously observed in polycrystalline Cr–Si alloys. Although the elastic constants also display structure effects at the I–C transition, it is worth noting that the I–C transition in the elastic constants is not smeared out over such a large temperature range ($\approx$ 35 K) as in the thermal expansion measurements ($\approx$ 60 K). Structure effects were absent, within the experimental error, on $(\Delta L/L)_{meas}$–T curves of Cr + 0.5 at.% Si and Cr + 1.6 at.% Si. No anomalies were observed down to 77 K for these two crystals, and also for Cr + 3.0 at.% Si, that could be identified with an I–C transition.

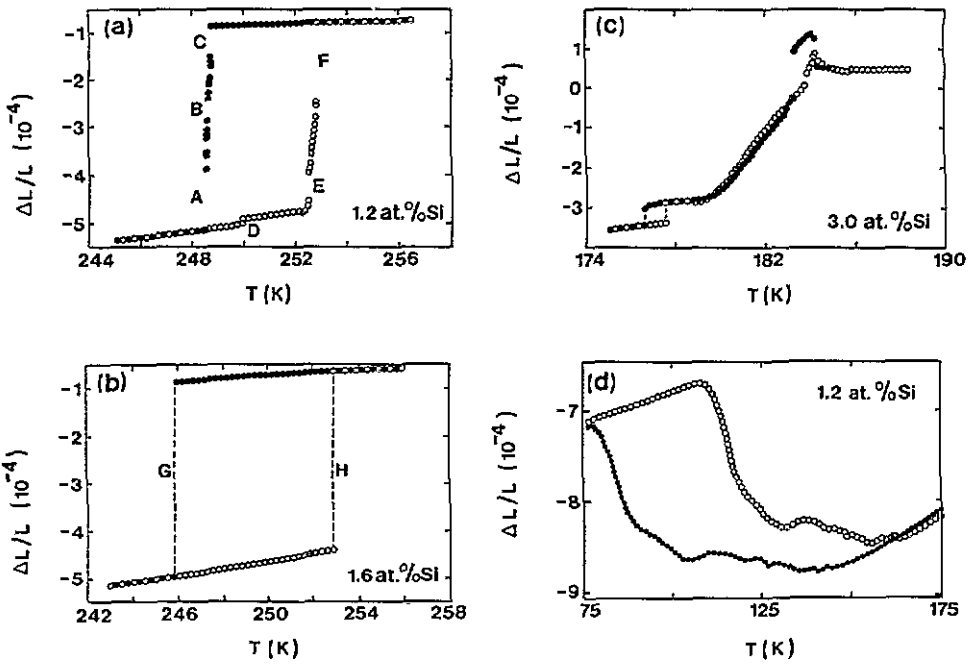

Figure 8. Detailed temperature behaviour of $\Delta L/L = (\Delta L/L)_{meas} = (\Delta L/L)_{Cr_{95}V_5} - (\Delta L/L)_{Cr-Si}$ measured along [100] around the Néel point, for (*a*) Cr + 1.2 at.% Si, (*b*) Cr + 1.6 at.% Si and (*c*) Cr + 3.0 at.% Si. The detailed behaviour of $\Delta L/L$ near T_{IC} is shown for the Cr + 1.2 at.% Si crystal in (*d*). Points marked o were recorded at temperature intervals smaller than 0.005 K during heating runs, and those marked • were measured at intervals smaller than 0.05 K during cooling runs. All the data points fall on smooth curves and only representative points are shown in the figures.

The thermal expansion of the Cr + 1.6 at.% Si crystal was also measured parallel to [110]. The results of the [100] and [110] measurements, within the experimental error, are the same, showing that this crystal is isotropic in its thermal expansion. This is assumed to be also the case for the other Cr–Si crystals. The magnetovolume is then given by

$$\Delta\omega = 3(\Delta L/L)_{meas} = 3[(\Delta L/L)_{Cr_{95}V_5} - (\Delta L/L)_{Cr-Si}]$$

and is obtained for 0.5 at.% Si, 1.2 at.% Si and 1.6 at.% Si from figure 7 by multiplying the $(\Delta L/L)_{meas}$ value at each temperature by a factor of three.

In figure 9 the coefficient of thermal expansion, α, is shown as a function of temperature for the Cr + 0.5 at.% Si, Cr + 1.2 at.% Si, Cr + 1.6 and Cr + 3.0 at.% Si crystals.

4. Discussion

The Néel temperatures obtained from the ultrasonic and thermal-expansion measurements on the Cr–Si single crystals compare fairly well with each other. The T_N of the single crystals in table 2 compares reasonably well with values of 276 K,

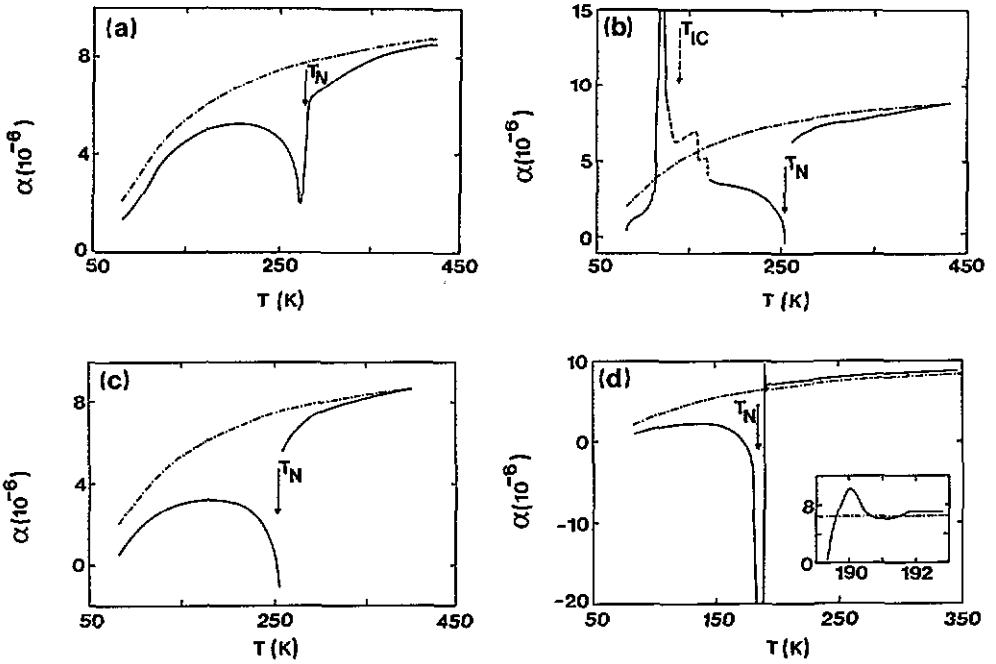

Figure 9. Coefficient of thermal expansion $\alpha = \mathrm{d}/\mathrm{d}T(\Delta L/L)_{\mathrm{Cr-Si}}$ for (*a*) Cr + 0.5 at.% Si, (*b*) Cr + 1.2 at.% Si, (*c*) Cr + 1.6 at.% Si and (*d*) Cr + 3.0 at.% Si measured along [100]. The smooth curves were drawn through the data points that were calculated as previously described [7] from the $\Delta L/L$ measurements. The scattering of the data points around the smooth curves are within 2–3%. The chain curves represent the expected non-magnetic behaviour given by α for Cr + 5 at.% V. In (*b*) the broken part of the curve reflects the structure observed in $\Delta L/L$ near T_{IC}. The inset in (*d*) gives the detailed behaviour near 190 K.

240 K, 242 K and 199 K obtained for 0.5 at.% Si, 1.2 at.% Si, 1.6 at.% Si and 3.0 at.% Si, respectively, from polycrystalline measurements taken during heating runs by Alberts and Lourens [3].

The first-order CSDW-P transitions observed for the Cr + 1.2 at.% Si and Cr + 1.6 at.% Si crystals were also observed [3,14] in thermal-expansion measurements on polycrystalline Cr–Si alloys near these concentrations. The measurements on the polycrystalline material, however, were only made during heating runs [3,14], and therefore do not reveal the hysteresis or structure effects reported in the present study on single crystals.

The concentration of the Cr + 1.2 at.% Si crystal is close to the triple-point concentration and in the region between 0.85 and 1.4 at.% Si where Mizuki and co-workers [2] predicted a re-entrant CSDW phase. From the predicted phase diagram of these authors, the Néel transition for Cr + 1.2 at.% Si should be a P-ISDW phase transition followed by a ISDW–CSDW transition at a temperature 8 K lower than T_N, and then by a CSDW–ISDW transition on further cooling through 164 K. Large and sharply defined discontinuities were observed in the $(\Delta L/L)_{\mathrm{meas}}$–$T$ curves of Cr + 1.2 at.% Si at T_N, as well as large anomalies when the C–I transition line around 150 K was crossed (figure 8). As the $(\Delta L/L)_{\mathrm{meas}}$ results were recorded continuously at 0.005 K intervals, one therefore expects signs of the transition from the ISDW phase

into the CSDW re-entrant phase on the measured $\Delta L/L$ curves of this crystal when cooled from above T_N.

Figure 8(*a*) shows the behaviour of $(\Delta L/L)_{meas}$ close to T_N for the 1.2 at.% Si crystal during both heating and cooling runs. A reproducible structure with discontinuities at D, E and F in the figure, is observed during the heating run in the transition region between 250K and 252.13K, indicating that the transition occurs in several steps between these two temperatures. A small reproducible minimum occurs between D and E on the heating run. This minimum, as well as the small discontinuity at D, were absent during repeated cooling runs, for which the transition is completed within 0.15K with sharp discontinuities at A, B and C (figure 8(*a*)). We reason that the structure effects observed during the heating cycle, but not during the cooling cycle, are probably not due to sample inhomogeneities. Such inhomogeneities will result in the transformation of parts of the crystal at different temperatures than other parts thereof, resulting in a smearing out of the transition and structure effects during both heating and cooling runs. A more likely explanation of these effects during the heating cycle is that they originate from mixed ISDW/CSDW states that probably exist in a small region of the magnetic phase diagram between the ISDW phase that occurs just below T_N and the re-entrant CSDW phase. It is thus suggested that the sequence of magnetic phases occuring during heating the Cr + 1.2 at.% Si crystal from 0K to high temperatures is: ISDW → mixed ISDW/CSDW → CSDW → mixed ISDW/CSDW → ISDW → P. This sequence accounts for structure effects on heating near T_N but not for its absence during cooling. Its absence during cooling is presumably due to supercooling directly into the re-entrant CSDW phase, thereby bypassing the very small regions of ISDW and mixed ISDW/CSDW states between T_N and the re-entrant phase, when the sample is slowly cooled through T_N. On the other hand, the first-order discontinuous transition observed in this crystal on both heating and cooling is characteristic of first-order CSDW-P transitions observed at T_N in Cr–Si [3,14] and Cr–Fe [15] alloys and not of ISDW-P transitions, which are usually continuous in Cr alloys [1]. The measurements on the Cr + 1.2 at.% Si crystal therefore indicate the possibility of a re-entrant CSDW phase, but do not settle this point fully. Careful neutron diffraction measurements on this crystal close to T_N are now needed to clarify this point.

As shown in figure 8(*b*), no structure effects were observed in the discontinuous transition, which is completed within 0.1K, for the Cr + 1.6 at.% Si crystal, indicating that it definitely lies above the triple point on the magnetic phase diagram.

Recently Galkin and co-workers [16] calculated the discontinuity $(\Delta L/L)_{T_N}$ in $(\Delta L/L)$ at T_N for dilute Cr–Si alloys by allowing for the effects of resonant impurity scattering and magnetostriction in the SDW model. They obtained (their figure 5) $(\Delta L/L)_{T_N} = 1.36 \times 10^{-4}$ and 1.54×10^{-4} respectively for Cr + 1.2 at.% Si and Cr + 1.6 at.% Si. The present measurements on the single crystals give for Cr + 1.2 at.% Si

$$(\Delta L/L)_{T_N} = \begin{cases} 3.97 \times 10^{-4} & \text{on heating} \\ 4.24 \times 10^{-4} & \text{on cooling} \end{cases}$$

and for Cr + 1.6 at.% Si

$$(\Delta L/L)_{T_N} = \begin{cases} 3.77 \times 10^{-4} & \text{on heating} \\ 4.04 \times 10^{-4} & \text{on cooling.} \end{cases}$$

The measured values are thus nearly three times larger than the theoretical results. We do not know the reason for this; however, note that polycrystalline measurements [15] give $(\Delta L/L)_{T_N} \approx 3.5 \times 10^{-4}$ for an alloy containing 1.2 to 1.3 at.% Si, $(\Delta L/L)_{T_N} \approx 4.5 \times 10^{-4}$ and 3.0×10^{-4} [14] for alloys containing 1.2 and 1.3 at.% Si, respectively, and $(\Delta L/L)_{T_N} \approx 3.7 \times 10^{-4}$ [3] for two polycrystalline alloys containing 1.42 and 1.79 at.% Si. These polycrystalline results agree rather well with the single-crystal measurements reported here.

The detailed behaviour of $(\Delta L/L)_{meas}$ near T_N for Cr + 3.0 at.% Si is shown in figure 8(*c*). The transition is smeared out between 176.5 K and 184.0 K showing structure effects between 176.5 K and 177.5 K as well as between 183.3 K and 184.3 K. These structure effects are present during both heating and cooling runs and are attributed to small inhomogeneities in this crystal. T_N for the Cr + 3.0 at.% Si crystal from the $\Delta L/L$ measurements was taken as midway between the above temperatures.

In analyzing the magnetic contribution to the bulk modulus and the magnetovolume we used a thermodynamic model that was previously successfully used for several Cr alloys [1, 17–19]. The main assumptions of the model are that the magnetic free energy is separable from the total free energy and that volume strain terms in the magnetic free energy dominate shear strain effects. The last assumption is nearly fully satisfied for the TISDW state of the Cr + 0.5 at.% Si crystal, and to a good approximation also for the CSDW states of the Cr + 1.6 at.% Si and Cr + 1.2 at.% Si crystals. As the CSDW state of the Cr + 1.6 at.% Si crystal exists from 252 K down to 77 K or below, and that of the Cr + 1.2 at.% Si crystal only from 250 K down to about 150 K, we analyzed the results for the ISDW phase of Cr + 0.5 at.% Si and for the CSDW phase of only Cr + 1.6 at.% Si.

Below T_N, but not in the limit $T \to T_N$, the magnetic free energy is written [17] as

$$\Delta F(t,\omega) = \phi(\omega) f(t(\omega))$$

where $\phi(\omega)$ depends on the volume strain ω. Here $f(t(\omega))$ is taken [17] as $f(t(\omega)) = (1 - t^2)^2$, where the reduced temperature is given by $t = T/T_0(\omega)$, with $T_0(\omega)$ a critical temperature parameter. It then follows [17] that

$$\Delta\omega = a_0 + a_1 t^2 + a_2 t^4 \tag{1}$$

$$\Delta B = b_0 + b_1 t^2 + b_2 t^4. \tag{2}$$

The constants (a_0, a_1, a_2) and (b_0, b_1, b_2) contain ϕ, its first and second derivatives (ϕ' and ϕ'') to strain as well as $\mathrm{d} \ln T_0/\mathrm{d}\omega$. Obtaining (a_0, a_1, a_2) and (b_0, b_1, b_2) from the measurements then allow for a determination of $\mathrm{d} \ln \phi/\mathrm{d}\omega$ and $\mathrm{d} \ln T_0/\mathrm{d}\omega$. In Steinemann's [1, 18, 20] handling of the thermodynamic model, T_0 is given by T_N, a situation that was found to be a good approximation in Cr–Fe alloys up to temperatures close to T_N [17]. In analyzing the Cr–Si data we will also use this approximation.

Figures 10(*a*), (*b*), (*c*) and (*d*) show the fit of equations (1) and (2) to the data for the ISDW phase of the Cr + 0.5 at.% Si crystal and the CSDW phase of the Cr + 1.6 at.% Si crystal. The fitting of equations (1) and (2) to the data is good up to temperatures fairly close to T_N, even for the Cr + 1.6 at.% Si crystal for which the CSDW-P transition at T_N is of first order. Values of (a_0, a_1, a_2) and (b_0, b_1, b_2) are

Table 3. Coefficients in the expansions $\Delta\omega(t) = a_0 + a_1t^2 + a_2t^4$ and $\Delta B(t) = b_0 + b_1t^2 + b_2t^4$ as well as values of $d \ln \phi/d\omega$ and $d \ln T_N/d\omega$ for Cr–Si alloys. The values of $d \ln \phi/d\omega$ shown in brackets are determined from values of (a_0, a_1, a_2) and those not in brackets from the values of (b_0, b_1, b_2).

at.% Si	$\Delta\omega = a_0 + a_1t^2 + a_2t^4$			$\Delta B = b_0 + b_1t^2 + b_2t^4$			$d \ln T_N/d\omega$	$d \ln \phi/d\omega$
	$a_0(\times10^{-3})$	$a_1(\times10^{-3})$	$a_2(\times10^{-3})$	$b_0(10^{11}\mathrm{Nm}^{-2})$	$b_1(10^{11}\mathrm{Nm}^{-2})$	$b_2(10^{11}\mathrm{Nm}^{-2})$		
0.5	-1.295 ± 0.004	0.264 ± 0.014	0.591 ± 0.013	0.120 ± 0.005	-0.040 ± 0.025	0.373 ± 0.025	45.5	(163) 89
1.6	-3.098 ± 0.002	1.266 ± 0.011	0.413 ± 0.010	0.342 ± 0.004	-0.116 ± 0.018	0.524 ± 0.019	54.0	(320) 125

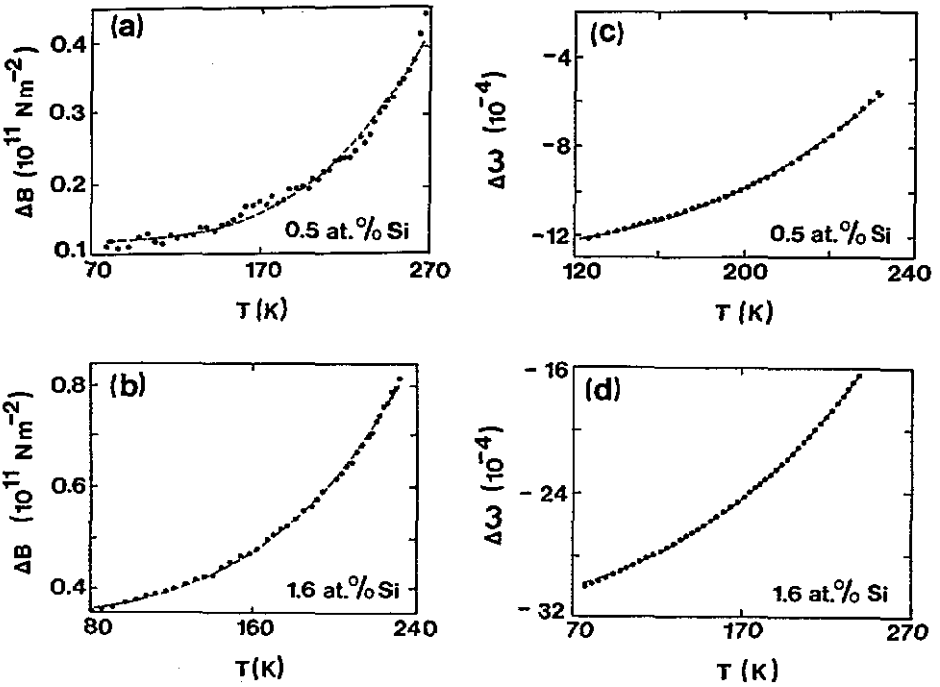

Figure 10. (*a*) and (*b*). The temperature dependence of the magnetic contribution to the bulk modulus, $\Delta B = B(\text{non-magnetic}) - B(\text{Cr} - \text{Si})$, for (*a*) Cr + 0.5 at.% Si and (*b*) Cr + 1.6 at.% Si. The broken curves are the best fits of the equation $\Delta B = B_0 + B_1T^2 + B_2T^4$. (*c*) and (*d*). The temperature dependence of the magnetovolume, $\Delta\omega$, for (*c*) Cr + 0.5 at.% Si and (*d*) Cr + 1.6 at.% Si. The broken curves, not everywhere equally visible since they follow the data points closely, are the best fits of the equation $\Delta\omega = A_0 + A_1T^2 + A_2T^4$.

tabulated in table 3 together with the values of $\mathrm{d}\ln\phi/\mathrm{d}\omega$ and $\mathrm{d}\ln T_N/\mathrm{d}\omega$, calculated using the same method as previously used [17] for Cr–Fe alloys.

From table 3 it follows that $a_1/a_0 + a_2/a_0 = -0.66$ and -0.53, respectively, for Cr + 0.5 at.% Si and Cr + 1.6 at.% Si. According to theory one should have $a_1/a_2 + a_2/a_0 = -1$. The measured values of -0.66 and -0.53 are close to the values obtained for Cr–Fe [17] and are in reasonable agreement with the value -1 if the approximations of the thermodynamic model are kept in mind.

The values of $\mathrm{d}\ln\phi/\mathrm{d}\omega$ calculated separately from (a_0, a_1, a_2) or (b_0, b_1, b_2) differ by a factor of up to three (table 3) as was also found [17] for Cr–Fe alloys. The discrepency may be attributed to the approximations in the thermodynamic model. The values of $\mathrm{d}\ln T_0/\mathrm{d}\omega \equiv \mathrm{d}\ln T_N/\mathrm{d}\omega$ are to be compared with direct measurements of Jayaraman and co-workers [21] on Cr–Si alloys. They obtained $\mathrm{d}\ln T_N/\mathrm{d}\omega \approx 31$–44 for Cr–Si alloys showing ISDW-P transitions and $\mathrm{d}\ln T_N/\mathrm{d}\omega \approx 123$–132 for alloys showing CSDW-P transitions. The value $\mathrm{d}\ln T_N/\mathrm{d}\omega = 45.5$ for Cr + 0.5 at.% Si of table 3 compares well with the directly measured result, but that of Cr + 1.6 at.% Si is lower by a factor between two and three.

Fawcett and Alberts [18] considered ϕ in the equation for $\Delta F(t, \omega)$ as a constant for the temperature regions $T \to T_N$ from above or below. This leads to the following Grüneisen parameters for these temperature regions:

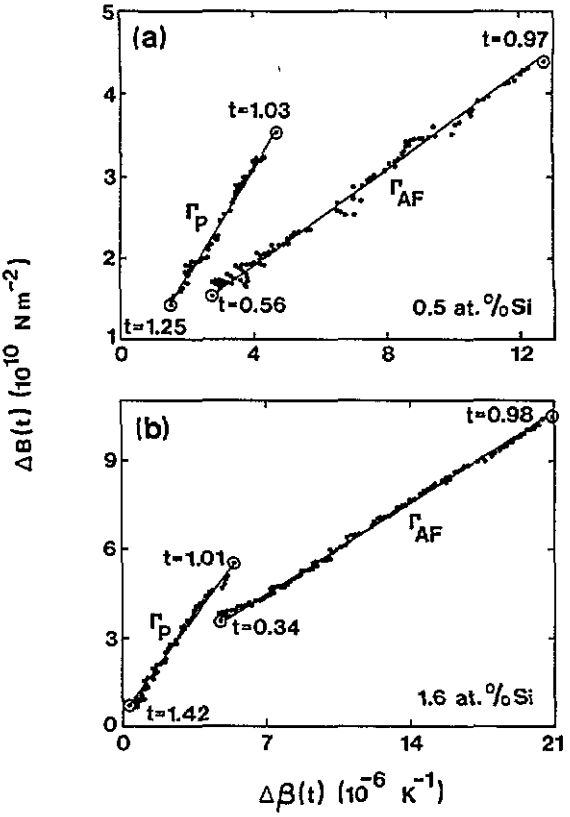

Figure 11. Graphs of the magnetic contributions to the bulk modulus, $\Delta B(t)$, as a function of the magnetic contribution to the volume thermal expansion coefficient, $\Delta\beta(t)$: (*a*) Cr + 0.5 at.% Si and (*b*) Cr + 1.6 at.% Si. For clarity, measurements are only shown in the linear regions of the plots. The curves are least-square fits to the data and the values of t at the encircled points are shown in the figures.

$$\Gamma_{AF} = -\mathrm{d}\ln T_N/\mathrm{d}\omega = -(1/T_N B)\lim_{t\to 1}(\Delta B/\Delta\beta) \qquad t < 1$$
$$\Gamma_P = -\mathrm{d}\ln T_{sf}/\mathrm{d}\omega = -(1/T_N B)\lim_{t\to 1}(\Delta B/\Delta\beta) \qquad t > 1. \tag{3}$$

The term T_{sf} is a spin fluctuation temperature, $\Delta\beta = 3\Delta\alpha$ is the magnetic contribution to the coefficient of volume thermal expansion, AF refers to the antiferromagnetic ($t < 1$) and P to the paramagnetic ($t > 1$) states, respectively. The requirement that Γ_{AF} and Γ_P be determined only in the limit $T \to T_N$ is not stringent [18]. Plots of $\Delta B(t)$ against $\Delta\beta(t)$, both above and below T_N, were found to be linear in a relatively wide temperature range near T_N for Cr, and Cr–Mo and Cr–Al alloys [18]. The terms Γ_{AF} and Γ_P are then determined from these linear parts. Figures 11(*a*) and (*b*) show results for Cr + 0.5 at.% Si and Cr + 1.6 at.% Si. The data fall on linear curves over a wide temperature range as shown in the figures, giving $\Gamma_{AF} = -56$ and $\Gamma_P = -133$ for 0.5 at.% Si, and $\Gamma_{AF} = -100$ and $\Gamma_P = -199$ for 1.6 at.% Si. For both alloys $|\Gamma_P| > |\Gamma_{AF}|$, showing that the short-range magnetic order and spin fluctuations above T_N are more volume dependent than the SDW below T_N. It is interesting to note that the linear relationship between $\Delta B(t)$ and

$\Delta\beta(t)$ holds for both Cr + 0.5 at.% Si, in which the transition at T_N is continuous, and for Cr + 1.6 at.% Si in which this transition is discontinuous.

5. Conclusions

The magnetoelastic properties of dilute Cr–Si single crystals were studied for the first time in alloys containing 0.5, 1.2, 1.6 and 3.0 at.% Si. For 0.5 at.% Si the transition at the Néel point is continuous, for 1.2 and 1.6 at.% Si it is first order with hysteresis, while the order of the transition in the 3.0 at.% crystal could not be determined unambiguously. Latent heat studies by Benediktson and co-workers [22] on Cr–Si alloys containing up to 1.85 at.% Si, suggest first-order Néel transitions in alloys containing 0.5, 1.2 and 1.6 at.% Si. This is consistent with the discontinuous transitions observed at T_N in the thermal expansion of the latter two crystals, but not with the observations of the first crystal, unless the transition is only weakly first order in it, as suggested by the very small latent heat [22] for this concentration. The 1.2 at.% Si crystal also show large hysteretic anomalies at the I–C and C–I transitions with the possibility of mixed ISDW/CSDW states near the I–C transition line at 150K in the magnetic phase diagram of Cr–Si alloys. It is speculated that the structure effects observed near T_N in the $(\Delta L/L)_{meas}$ curves of the Cr + 1.2 at.% Si crystal, and also in its elastic constants, are signs of the re-entrant CSDW phase predicted by Mizuki and co-workers [2]. The suggested sequence of phase changes in this crystal on heating from 0K, is from ISDW to mixed ISDW/CSDW to CSDW to mixed CSDW/ISDW back to ISDW and then to P. Careful neutron diffraction experiments are needed on this crystal to verify this sequence. All elastic constants show anomalies at the spin-flip and I–C transition temperatures, something that was not previously observed in measurements on polycrystalline Cr–Si alloys. The magnetoelastic properties of the Cr + 0.5 at.% Si and Cr + 1.6 at.% Si crystals are described reasonably well by the thermodynamic model, giving acceptable values of $\mathrm{d}\ln\phi/\mathrm{d}\omega$ and $\mathrm{d}\ln T_N/\mathrm{d}\omega$.

Acknowledgments

Financial aid from the Foundation for Research Development is acknowledged, as well as technical assistance from T Germishuyse and S I Wagener. RAA would like to thank the Rand Afrikaans University for the hospitality enjoyed during his visit.

References

[1] Fawcett E, Alberts H L, Galkin V Yu, Noakes D R and Yakhmi J V 1993 *Rev. Mod. Phys.* at press
[2] Mizuki J, Copley J R D, Endoh Y and Ishikawa Y 1986 *J. Phys. F: Met. Phys.* **16** L195
[3] Alberts H L and Lourens J A J 1988 *J. Phys. F: Met. Phys.* **18** 123
[4] Alberts H L and Boshoff A H 1992 *J. Magn. Magn. Mater.* **104-107** 2031
[5] Bohlmann M and Alberts H L 1970 *J. Phys. E: Sci. Instrum.* **3** 779
[6] Papadakis E P 1976 *Physical Acoustics* vol XII, ed W P Mason and R N Thurston (New York: Academic)
[7] Alberts H L and Lourens J A J 1984 *Phys. Rev.* B **29** 5279
[8] Alberts H L 1990 *J. Phys.: Condens. Matter* **2** 9707
[9] Truell R, Elbaum C and Chick B B 1969 *Ultrasonic Methods in Solid State Physics* (New York: Academic)

[10] Elliot R P 1965 *Constitution of Binary Alloys* (first suppl.) (New York: McGraw-Hill)
[11] Van Rijn H J and Alberts H L 1983 *J. Phys. F: Met. Phys.* **13** 1559
[12] Lourens J A J and Alberts H L 1993 *Int. J. Mod. Phys.* B at press
[13] Booth J G, Costa M M R, Rodriguez-Carjaval J and Paixao J A 1992 *J. Magn. Magn. Mater.* **104–107** 735
[14] Suzuki T 1977 *J. Phys. Soc. Japan* **43** 869
[15] Fawcett E and Galkin V Yu 1992 *J. Magn. Magn. Mater.* **109** L139
[16] Galkin V Yu, Tugushev V V and Tugusheva T E 1991 *Sov. Phys.–Solid State* **33** 4
[17] Alberts H L and Lourens J A J 1992 *J. Phys.: Condens. Matter* **4** 3835
[18] Fawcett E and Alberts H L 1990 *J. Phys.: Condens. Matter* **2** 6251
[19] Fawcett E and Alberts H L 1992 *J. Phys.: Condens. Matter* **4** 613
[20] Steinemann S G 1978 *J. Magn. Magn. Mater.* **7** 84
[21] Jayaraman A, Maines R G, Rao K V and Arajs S 1976 *Phys. Rev. Lett.* **37** 926
[22] Benediktsson G, Hedman L, Åström H U and Rao K V 1982 *J. Phys. F: Met. Phys.* **12** 1439